COMMUNICATIONS IN SCIENCE AND TECHNOLOGY
Homepage: cst.kipmi.or.id

Synthesis and characterization of hydroxyapatite/SiO_2/gelatin composites as bone scaffold candidates

Indah Wahda, Syahruddin Kasim, Maming, Hasnah Natsir, St. Fauziah, Yusafir Hala, Andi Muhammad Anshar, Andriani Usman, Windasari, Indah Raya*

Department of Chemistry, Hasanuddin University, Makassar 90245, Indonesia

Article history:
Received: 12 December 2023 / Received in revised form: 24 February 2024 / Accepted: 16 May 2024

Abstract

This study aims to determine the characteristics of hydroxyapatite/SiO_2/gelatin composites to fulfil the bone scaffold standards. XRF analysis showed that limestone has a high CaO content of 92.89%, allowing it be used for hydroxyapatite synthesis. The wet precipitation method was used to synthesize hydroxyapatite; meanwhile, the freeze-drying method was used to synthesize the hydroxyapatite/SiO_2/gelatin scaffold. FTIR analysis confirmed the characteristic peaks, which indicated the presence of compounds of hydroxyapatite (OH^- and PO_4^{3-}), SiO_2 (Si-OH and Si-O-Si), and gelatin (N-H, C-H, and C=O). XRD analysis showed 98.1% hydroxyapatite phase and 1.9% SiO_2 phase and SEM analysis showed a scaffold pore size of 155-218μm, optimal for cell attachment. Furthermore, mechanical testing resulted in a compressive strength of 1.71 MPa and porosity testing resulted in a porosity of 75%. This characterization showed the potential use of hydroxyapatite/SiO_2/gelatin composites as bone scaffolds. This research can enable further development of scaffold materials in the field of tissue engineering.

Keywords: Limestone; hydroxyapatite/SiO_2/gelatin; scaffold

1. Introduction

Osteoporosis is a bone disorder that currently becomes a widespread problem, as its incidence rate increases rapidly with age. More than 200 million people are thought to have osteoporosis at this time [1]. Increasing bone density or using appropriate materials to fill bone defects are two ways to overcome osteoporosis [2]. Several therapies for fracture healing are clinically established but they still have several drawbacks, such as donor difficulties, cost, time, safety, and the inability to fix significant bone abnormalities. Effective regeneration therapies are therefore required to restore physiological appearance and function and produce long-lasting effects [3].

Bone scaffold fabrication is currently widely developed in medicine field for tissue engineering [4]. Scaffold has an advantage as a medium that promotes the formation of new bone derived from the patient's stem cells, fully integrated with the existing skeletal system [3]. As tissue engineering media, it is expected to have good biocompatibility, biodegradability, bioabsorbability, and bioactivity and possess appropriate structural qualities like strong mechanical strength, high porosity, and pore interconnectivity [5]. One of the biomaterials used in scaffold development is hydroxyapatite.

Hydroxyapatite ($Ca_{10}(PO_4)_6(OH)_2$) is a bioactive calcium phosphate compound that has a main constituent component that resembles real bone. It is non-toxic and has good bioactivity, biocompatibility, bioabsorbability, osteoconductivity, and chemical stability properties. For this, hydroxyapatite is widely applied in biomedical applications [6,7,8]. In addition, hydroxyapatite is a biomaterial that has a great potential as a scaffold; however, its biological activity is limited in several applications due to factors such as particle migration from the implant region and mechanical brittleness, which significantly restricts its use in bone tissue engineering [8,9] Therefore, the development of hydroxyapatite-based materials has led to doped or composite hydroxyapatite materials. Silicon oxide (SiO_2) is one of the effective particle-mediated reinforcing materials that has attracted much attention. Adding SiO_2 to hydroxyapatite can greatly increase the bonding strength of hydroxyapatite particles [10]. Therefore, compositing hydroxyapatite with SiO_2 is able to improve the material's mechanical strength [11].

The ability of hydroxyapatite as a scaffold can be maximized by compositing with gelatin - a collagen-derived biopolymer that has biocompatible, biodegradable, non-toxic, and non-immunogenic properties [12]. Gelatin has some properties allowing for variations in cell adhesion and proliferation and improving the biological properties of

* Corresponding author. Tel: +62. 822-9116-9609
Email: indahraya@unhas.ac.id
https://doi.org/10.21924/cst.9.1.2024.1350

polymeric devices after implantation [13]. It is also considered effective in modifying the properties of hydroxyapatite for being a biopolymer that can develop pore structures to boost surface area and produce gaps that help injured bones to absorb nutrients and support cell development [3].

Based on the description of the problems in the background, this research aims to synthesize hydroxyapatite using limestone base material and reinforce it with SiO_2 and gelatin to improve the mechanical properties, pores, and porosity of hydroxyapatite.

2. Materials and Methods

2.1. Preparation of limestone

Limestone samples were washed and cleaned prior to be mashed and dried for 2 hours at 110ºC in the oven. Then, it was sieved with a size of 100 mesh in order to produce limestone powder that, later on, was analyzed with FTIR. Furthermore, limestone powder was calcined in a furnace at 1000ºC for 5 hours [14]. The calcined limestone powder subsequently was analyzed by XRF and FTIR.

2.2. Preparation of calcium solution and phosphate solution

The preparation of the calcium solution precursor was carried out by weighing CaO powder from calcined limestone as much as 5.6 g and mixing it with 100 mL of aquabides [15]. The solution was stirred using a magnetite stirrer for 2 hours at 40ºC to produce a 1 M $Ca(OH)_2$ solution [16]. Furthermore, a 0.6 M phosphoric acid (H_3PO_4) solution was made. A total of 4.1 mL of 85% phosphoric acid was added to aquabides until the volume reached 100mL. The solution was shaken until homogeneous to obtain 100mL of (H_3PO_4) 0.6 M [15].

2.3. Synthesis of hydroxyapatite

Synthesis of hydroxyapatite was carried out by mixing a calcium solution with a phosphoric acid solution. It was done through the titration method by dripping 100 mL of H_3PO_4 solution into 100 mL of $Ca(OH)_2$ suspension with a flow rate of 1 mL/minute [15]. The mixing was carried out while stirring using a magnetic stirrer at 40ºC (kept constant) until the H_3PO_4 ran out in the titration process [14]. Once the H_3PO_4 ran out in the titration process, the mixture was heated at 60ºC for 1 hour, and NaOH was added until reaching pH 10 [15].

The suspension was left at room temperature for 24 hours. Next, the resulted precipitate was filtered and washed with aquabides before being dried for 2 hours at 110°C to get rid of any last traces of aquabides from the washing [14]. The sample was pulverized then. It was continued by conducting calcination at 900ºC within 6 hours [15]. At last, the resulted hydroxyapatite powder was analyzed by XRD to determine the main phase and purity of hydroxyapatite and continued with FTIR characterization to identify functional groups [17].

2.4. Synthesis of hydroxyapatite/SiO_2 composites

Hydroxyapatite/SiO_2 composite synthesis was carried out by mixing hydroxyapatite with SiO_2 at a ratio of 90:10. Here, hydroxyapatite was the matrix and SiO_2 was the filler in this scaffold composite. The amount of hydroxyapatite was more dominant for being the main component of bone requiring the modification of its mechanical properties. The addition of SiO_2, meanwhile, aimed to improve the mechanical strength of hydroxyapatite. However, the composition of SiO_2 should not be excessive to prevent that it could interfere with porosity, which is also important for bone cell growth [18]. Next, the sample hydroxyapatite/SiO_2 was dissolved with aquabides and stirred until being well mixed. It was then filtered using a vacuum pump. In the end, the resulted sample was oven-dried at 110ºC for 3 hours to produce hydroxyapatite/SiO_2 powder [19].

2.5. Synthesis of scaffold hydroxyapatite/SiO_2/gelatin

Gelatin weighing as much as 1.4 g was dissolved with aquabides and heated at 40ºC with continuous stirring for 10 minutes. 2 g of hydroxyapatite/SiO_2 composite powder was then added to the solution with constant stirring for 40 minutes to obtain a homogeneous mixture [20]. Following this, the resulted slurry (Hydroxyapatite/SiO_2/Gelatin) was molded using a tube-shaped mold. The molded mixture was frozen before being freeze-dried. Freezing here was carried out at -20ºC for 24 hours. Furthermore, the frozen samples were lyophilized using freeze-drying for 52 hours at -52ºC. Furthermore, it was analyzed using FTIR, XRD, SEM, mechanical tests, and porosity tests.

2.6. Characterization with fourier transform infrared (FTIR)

Characterization using FTIR was conducted to identify the functional groups in each composite scaffold compound. The samples were measured using Shimadzu-type IRPrestige-21. The sample to be analyzed was mixed with KBr powder in a mortar, and pressed to form a pellet. It was then measured using an FTIR spectrophotometer in the wave number range 4000-350 cm^{-1}.

2.7. Characterization with X-Ray diffraction (XRD)

Characterization using XRD was performed to identify the phase and crystalline nature of the composite scaffold. The samples were characterized using a SHIMADZU 7000 XRD tool at an angle of 2θ: 15°-70° with a current of 30 mA and a voltage of 40 kV with a Cu-Kα radiation source (λ =1.54056 Å). The XRD results were in the form of phase graphs identified based on the intensity and 2θ angle formed. The phase determination here referred to the Joint Committee on Powder Diffraction Standard (JCPDS).

2.8. Characterization with electron microscopy spectroscopy (SEM)

Characterization using SEM aimed to see the surface morphology and pore size of the sample. The samples were characterized using a JEOL tool type JCM6000Plus and were placed on the aluminum block with a diameter of 25 mm. The

samples were then observed using SEM with a voltage of 15 kV.

2.9. Mechanical test

The mechanical test of the sample was done by performing conducting a compressive strength test using a universal testing machine at room temperature. The sample was cut into a certain size and was mounted on a pedestal found on the machine. Subsequently, it was pressed by paying attention to the reading on the measuring instrument until it reached the maximum compressive force. The results obtained were displayed on the computer connected to the tool.

2.10. Porosity test

The porosity of the hydroxyapatite/SiO_2/gelatin scaffold was measured using the liquid displacement method. The scaffold was immersed in an ethanol solution of known volume and recorded as (Va), and the combined volume of scaffold and ethanol was noted as (Vb). The scaffold was soaked for 48 hours and removed from the ethanol solution. The volume of ethanol, after the scaffold was taken away, was recorded as (Vc) [21]. The porosity of hydroxyapatite/SiO_2/gelatin scaffolds can be calculated using the formula in Equation 1.

$$\%Porosity = \left(\frac{Va - Vc}{Vb - Vc}\right) \times 100\% \quad (1)$$

3. Results and Discussion

3.1. Calcination of limestone

Limestone is a mineral that has a high CaO content because it has gone through a $CaCO_3$ decomposition process. This makes it a potential precursor for hydroxyapatite synthesis. The hydroxyapatite synthesis process begins with the calcination of limestone. The calcination aims to produce calcium oxide (CaO) crystals from calcium carbonate ($CaCO_3$) molecules [22]. When $CaCO_3$ compounds receive heat, their atoms move faster and breaks the chemical bonds of $CaCO_3$ into CaO and CO_2 [23]. In this study, the sample was calcined at 1000ºC for 5 hours and successfully converted $CaCO_3$, as evidenced by the results of the FTIR analysis of limestone before and after calcination in Fig. 1. The $CaCO_3$ decomposition reaction is shown in Equation 2.

$$CaCO_3 \longrightarrow CaO + CO_2 \quad (2)$$

As shown in Fig. 1, FTIR identification showed some changes in the IR spectrum of limestone samples before and after calcination. In the limestone sample after calcination, there was a process of decomposition of $CaCO_3$ into CaO, characterized by the loss of CO_3^{2-} vibrations and the appearance of Ca-O vibrations in the samples as presented in Table 1. This occurred due to heating at high temperatures. While for the sample before calcination, there was still a CO_3^{2-} group. The CO_3^{2-} limestone cluster before calcination appeared at certain wave numbers. This data demonstrated that calcium in the form of calcite predominated in limestone prior to calcination, as characterized by the presence of CO_3^{2-} main vibrations. A research by Klinkaewnarong and Songkot [24] showed that in limestone samples before calcination, three CO_3^{2-} vibrations occurred around 1400, 875, and 711 cm^{-1} ascribed to asymmetric stretching (υ_3), out-of-plane bending (υ_2), and in-plane bending (υ_4). In addition, OH^- vibrations also appeared in the samples before and after calcination. This is in accordance with the research of Kumar et al. [25] who found that the sharp peak at wave number 3641 cm^{-1} appearing in the calcined sample was OH^- vibration. Table 1 groups the results of the FTIR analysis of limestone before and after calcination.

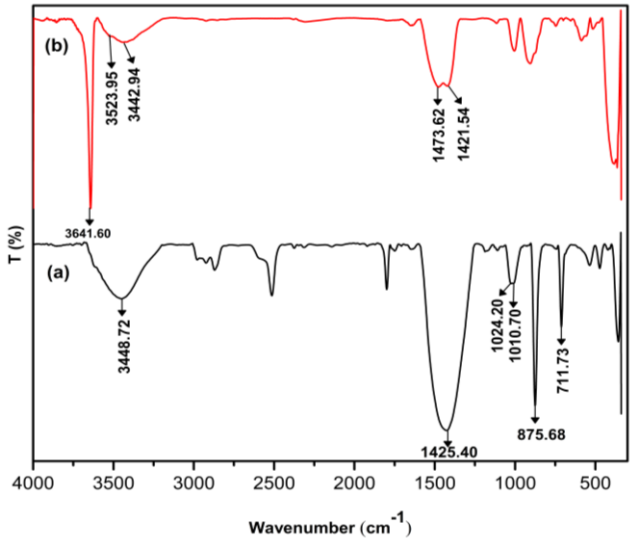

Fig. 1. FTIR spectra of limestone a) Before calcination b) After calcination

Table 1. Results of FTIR analysis of limestone before and after calcination

Vibration		Wavenumber (cm^{-1})	
		Before calcination	After calcination
OH^-		3448.72	3641.60,3523.95 and 3442.94
CO_3^{2-}	υ_1	1024.20 and 1010.70	-
	υ_2	875.68	-
	υ_3	1425.40	-
	υ_4	711.73	-
Ca-O		-	1473.62 and 1421.54

The calcined limestone samples were then analyzed using X-ray fluorescence (XRF) to prove the phase changes occurred and the results can be seen in Table 2. XRF data showed that the dominant compound in limestone was CaO, with a percentage of about 92.89%. The high percentage of CaO content obtained indicated that the calcined limestone has been completely converted from the $CaCO_3$ phase to CaO. This made calcined limestone to have great potential as a calcium precursor in hydroxyapatite synthesis. Based on XRF data, limestone after calcination also had a SiO_2 content of 5.6% that had no effect on the hydroxyapatite synthesis process or in the composite synthesis process. In the process

of hydroxyapatite synthesis, what occurs is the interaction between calcium ions from calcium oxide precursors with phosphate ions to form apatite compounds in accordance with hydroxyapatite stoichiometry. As SiO_2 is not part of the apatite crystal structure, its presence has no effect on the formation of the resulting compound. Table 2 presents the results of sample analysis by XRF.

Table 2. Limestone content

Parameters	Results (m/m%)
CaO	92.89
SiO_2	5.86
Fe_2O_3	1.2
Nb_2O_5	0.016
MoO_3	0.0125

3.2. Synthesis of hydroxyapatite

In this study, the wet precipitation method was used to synthesize hydroxyapatite compounds in which the material reacted in an aqueous medium without any solvents that had toxic properties [26]. Hydroxyapatite was synthesized using CaO from limestone as a calcium precursor and phosphoric acid as a phosphate precursor. The calcination of limestone formed a CaO compound, which was then dissolved with water to form $Ca(OH)_2$ [27]. The two precursors were mixed at a temperature of 40°C with a flow rate of 1 mL/min. The temperature and rate of addition of reactants determined the size and shape of the particles [26]. The mixture was then precipitated with an aging time of 24 hours to obtain a precipitate, which was again calcined to obtain hydroxyapatite compounds. Hydroxyapatite formation occurred based on Equation 3.

$$10Ca(OH)_2 + 6H_3PO_4 \longrightarrow Ca_{10}(PO_4)_6(OH)_2 + 18H_2O \quad (3)$$

3.3. Characterization of hydroxyapatite with fourier transform infrared (FTIR)

As shown in the FTIR spectrum in Fig. 2, the absorption peak of hydroxyapatite was visible in the wave number range of 300 cm^{-1}-4000 cm^{-1}. Analysis with FTIR on hydroxyapatite samples aimed to identify functional groups in hydroxyapatite compounds, which generally are hydroxyl and phosphate [28]. The peaks at wave numbers 3568.31 cm^{-1} and 3446.79 cm^{-1} were hydroxyl (OH^-) stretching modes, which are free and bound OH^- groups, respectively. Phosphate (PO_4^{3-}) vibrations were detected at wave numbers 1091.71 and 1043.49 cm^{-1} (υ_3), 960.55 cm^{-1} (υ_1), 632.65, 603.72, and 570.93 cm^{-1} (υ_4), and 366.48 cm^{-1} (υ_2).

The results obtained are supported by the research of Raya et al. [29], which also synthesized hydroxyapatite and results obtained were not much different showing the PO_4^{3-} group at wave numbers of 1120.64 cm^{-1}, 1091.71 cm^{-1}, 1043.49 cm^{-1} (υ_3), and 993. 34 cm^{-1}, 877.61 cm^{-1} (υ_1), 603.72 cm^{-1}, 565.14 cm^{-1} (υ_4), and 370.33 cm^{-1} (υ_2). For OH^- groups, there was a sharp spectrum at wave number 3570.24 cm^{-1} indicating the presence of free OH^- and 3427.51 cm^{-1} indicating bound OH^-. Emami et al. [26] also reported that the characterization of hydroxyapatite powder had a peak in the range of 560-610 cm^{-1} associated with asymmetric bending vibrations of PO_4^{3-}, in addition to peaks appearing in the range of 962 cm^{-1} and 1100-1000 cm^{-1} associated with asymmetric stretching vibrations of PO_4^{3-}, and found a peak in the 3572 cm^{-1} region associated with OH^- stretching vibrations. The hydroxyl group was characterized by a characteristic peak at 3800-3200 cm^{-1} originating from hydrated inorganic compounds, which was likely derived from the infiltrated water content during hydroxyapatite production. Water in combination with the crystal structure of the material causes stretching and bending of the OH^- bond and produces a peak at that position [28]. The results of the IR spectra confirmed that all prepared samples had phosphate and hydroxyl functional groups, indicating the formation of hydroxyapatite compounds [30].

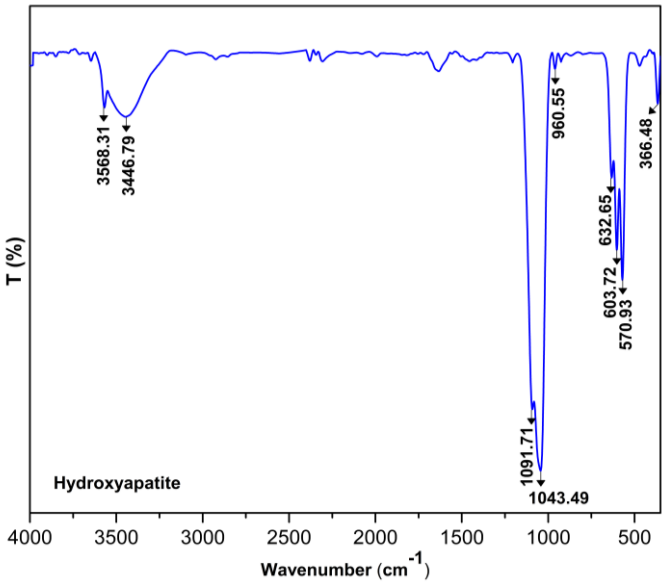

Fig. 2. FTIR spectra of limestone hydroxyapatite

3.4. Characterization of SiO_2 with fourier transform infrared (FTIR)

The results of the characterization of SiO_2 samples using FTIR are shown in Fig. 3 in the range of wave numbers 300 cm^{-1}–4000 cm^{-1}. As shown in the Fig., there were visible peaks of functional groups that represented the compounds formed. The results obtained showed the characteristics of SiO_2, characterized by the formation of peaks of silanol groups (Si-OH) and siloxane (Si-O-Si). The peak at wave number 3441.01 cm^{-1} had OH stretch vibrations, included in the Si-OH group. The peaks at wave numbers 1087.85 cm^{-1} and 1014.56 cm^{-1} were asymmetric Si-O-Si stretching vibrations, and at wave numbers 487.99 cm^{-1} and 443.63 cm^{-1} there were Si-O bending vibrations, which are also a group of Si-O-Si groups.

The results obtained are supported by the research of Nayak and Datta. [31], stating that the dominant functional groups in silica samples were silanol and siloxane, which occurred at the wave number 3430.31 cm^{-1} representing the O-H vibration in the Si-OH group, at wave numbers 1100.69 cm^{-1} and 1090.57 cm^{-1} which were asymmetric Si-O-Si strain vibrations, and at wave numbers 468.14 cm^{-1} and 460.43 cm^{-1}

which were Si-O bending vibration. Similar results were also reported in research conducted by Nazopatul et al. [32], who obtained results that in commercial SiO_2 samples there was a silanol functional group (Si-OH) at a wave number of 3384.25 cm^{-1} and absorption of a siloxane functional group (Si-O-Si) with an asymmetric strain mode at a wave number of 1095.65 cm^{-1} and there were Si-O bending vibrations occurred at the wave number 483.39 cm^{-1} also as a group of Si-O-Si groups. Therefore, the formation of absorption of silanol groups (Si-OH) and siloxane groups (Si-O-Si) showed that these groups are the main characteristics of SiO_2 compounds [32].

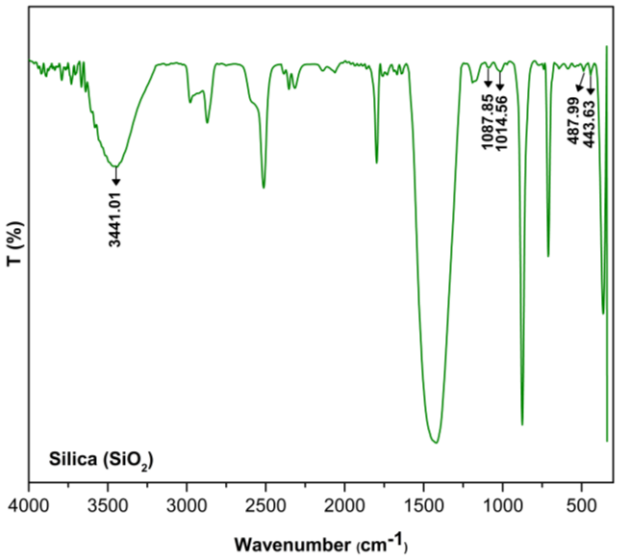

Fig. 3. FTIR spectra of SiO_2

3.5. Characterization of gelatin with fourier transform infrared (FTIR)

The results of gelatin sample characterization using FTIR are shown in Fig. 4 in the wave number range of 300 cm^{-1}-4000 cm^{-1}. Five common absorptions for gelatin samples, namely amides A, B, I, II, and III are displayed in the FTIR spectrum results. The amide A absorption was found at wave number 3456.44 cm^{-1} which is an N-H stretching vibration due to the presence of hydrogen bonds in the gelatin molecule [33]. Amide B absorption was found at wave number 2927.94 cm^{-1} which is an asymmetric vibration of C-H. Amide I absorption was at wave numbers 1654.92 cm^{-1} and 1631.78 cm^{-1} which is a C=O stretching vibration. Meanwhile, Amide II was found at wave number 1435.04 cm^{-1} which is N-H bending and Amide III absorption was at wave number 1240.23 cm^{-1} which is N-H bending vibrations.

Similar results have been reported in the research of Wahyuningtyas et al. [34] showing that amide A was absorbed at wave numbers 3525-3356 cm^{-1} which showed N-H stretching, and amide B was absorbed at wave numbers 2960-2874 cm^{-1} representing C-H vibrations, the amide I region was absorbed at wave numbers 1683-1631 cm^{-1} representing C=O stretch vibrations, amide II region was absorbed at wave numbers 1548-1442 cm^{-1} associated with a combination of C-N stretching and N-H bending of peptide groups and amide III region was absorbed at wave numbers 1269-1080 cm^{-1} associated with a combination of C-N stretching and N-H bending peaks.

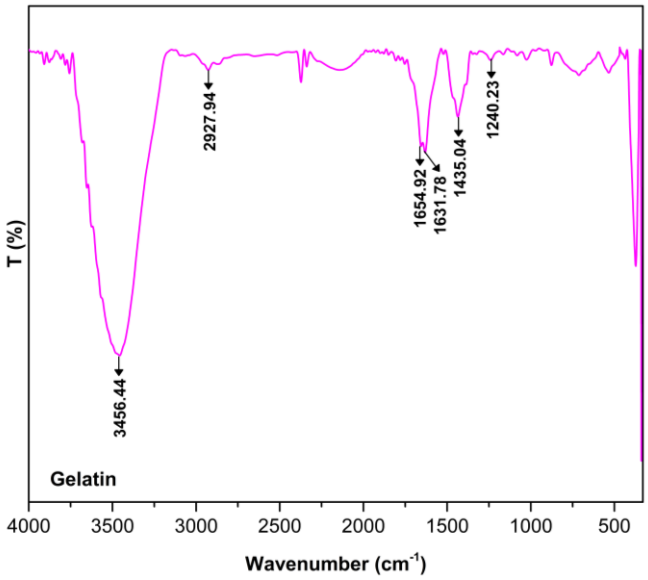

Fig. 4. FTIR spectra of gelatin

3.6. Characterization of hydroxyapatite/SiO_2/gelatin scaffolds with fourier transform infrared (FTIR)

In Fig. 5(a), the hydroxyapatite/SiO_2 composites absorption peaks were visible in the FTIR spectrum. The hydroxyapatite/SiO_2 composite was successfully carried out, which was characterized by the appearance of typical peaks for each compound. The hydroxyapatite phase was formed, characterized by the presence of PO_4^{3-} groups at wave numbers 1093.64 and 1041.56 cm^{-1} (υ_3), 960.55 cm^{-1} (υ_1), 632.65, 603.72 and 570.93 cm^{-1} (υ_4) and 364.55 cm^{-1} (υ_2), and OH^- groups at wave numbers 3572.17 and 3433.29 cm^{-1} that was in accordance with the typical peak of the sample before the composite. The typical peak of SiO_2 was also visible in the sample after the composite, namely the formation of a small absorption peak of the siloxane group at wave numbers 472.56 cm^{-1} and 412.77 cm^{-1}.

The hydroxyapatite/SiO_2/gelatin scaffold absorption peaks were visible in the FTIR spectrum as displayed in Fig. 5b. The hydroxyapatite/SiO_2 composite was successfully carried out, which was also characterized by the appearance of typical peaks for each compound. The PO_4^{3-} group from hydroxyapatite remained visible at a typical wave number as it was before the composite. Absorption for SiO_2 was also seen at the wave number 422.41 cm^{-1} with a small intensity. Other absorptions that were also formed represented gelatin at wave numbers 2931.80 and 2875.86 cm^{-1} i.e. asymmetric C-H vibrations for the absorption of amide B gelatin. Apart from that, C=O vibrations at wave number 1660.71 cm^{-1} represented amide I absorption. Peaks at wave numbers 1554.63 and 1452.40 cm^{-1} that were N-H vibrations for amide II gelatin absorption, and amide III gelatin absorption also appeared at wave number 1240.23 cm^{-1} associated with N-H vibrations.

Based on FTIR data (Fig. 5(a)), chemical interaction occurred in the hydroxyapatite/SiO_2 composite through the formation of hydrogen bonds between the hydroxyl group (OH^-) of hydroxyapatite and the silanol group (Si-OH) of silica, as characterized by a shift in the absorption band of the

hydroxyl group of hydroxyapatite and the absence of the Si-OH peak after composite. The loss of Si-O-Si group absorption in the FTIR spectrum of the hydroxyapatite/SiO_2 composite also proved the occurrence of chemical interactions between hydroxyapatite and silica. In the hydroxyapatite/SiO_2/gelatin composite, chemical interactions also occurred between the gelatin functional group (N-H) and the hydroxyl group (O-H) of hydroxyapatite through the formation of hydrogen bonds, as shown by the widening absorption peak at the wave number 3479.58 cm^{-1} (Fig. 5(b)).

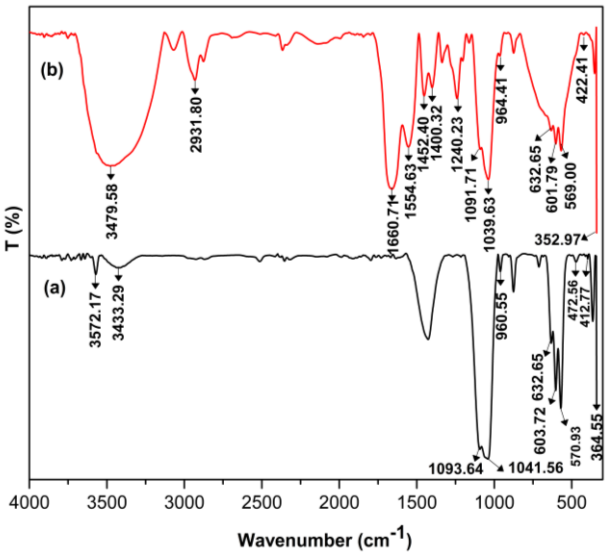

Fig. 5. FTIR spectra a) Hydroxyapatite/SiO_2 b) Hydroxyapatite/SiO_2/gelatin

3.7. Characterization of hydroxyapatite with X-Ray diffraction (XRD)

X-ray diffraction (XRD) characterization was carried out to determine the phase and purity of the synthesized calcium-phosphate compounds. The XRD pattern (Fig. 6) was compared to the standard hydroxyapatite data (JCPDS No. 9002216). Based on the diffractogram, the three highest intensity peaks were observed at 2θ values of 31.8264°, 31.0737°, and 32.8357°, corresponding to crystalline hydroxyapatite. This indicated that hydroxyapatite was the predominant calcium-phosphate phase obtained.

Further analysis of the XRD data using Origin software revealed 98% purity of the hydroxyapatite phase with a hexagonal crystal structure. The remaining 2% was identified as fluoroapatite. The presence of this minor fluoroapatite phase did not alter the bioactive properties of hydroxyapatite, owing to the similar chemical structures and characteristics of the two compounds. Moreover, fluoroapatite possesses favorable chemical stability and crystal structure, making it compatible for hydroxyapatite-based bone scaffold development [35]. Table 3 shows the highest peaks of hydroxyapatite samples.

Table 3. Angle 2θ of synthesized hydroxyapatite

	Crystal plane (hkl)				
	(002)	(121)	(300)	(202)	(301)
Hydroxyapatite	25.7430	31.0737	31.8264	32.8357	35.1200

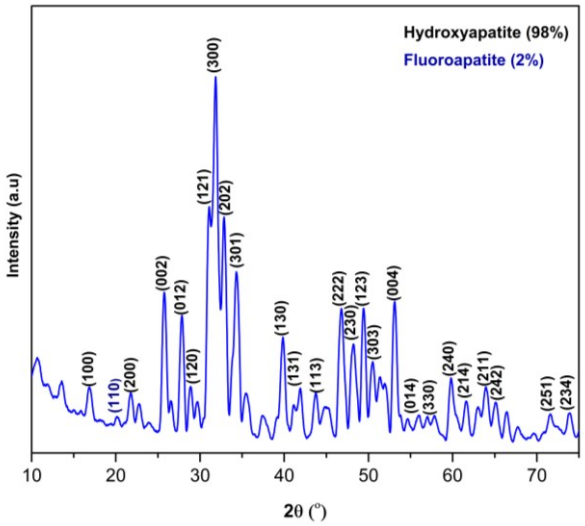

Fig. 6. Diffraction pattern of limestone hydroxyapatite

3.8. Characterization of hydroxyapatite/SiO_2/gelatin scaffolds with X-Ray diffraction (XRD)

The XRD pattern of the hydroxyapatite/SiO_2/gelatin scaffold is shown in Fig. 7. Based on the XRD pattern of hydroxyapatite/SiO_2/gelatin scaffold samples, the phase formed was dominated by hydroxyapatite with a purity of 98.1%, followed by the SiO_2 phase with a purity of 1.9%. The highest 2θ angle peaks showed the hydroxyapatite phase occurred at 32.2240 (121), 33.2422 (300), and 64.3933 (233). As for the SiO_2 phase, it appeared at 2θ angles of 29.5050 (111), 45.5150 (334), and 56.1800 (113).

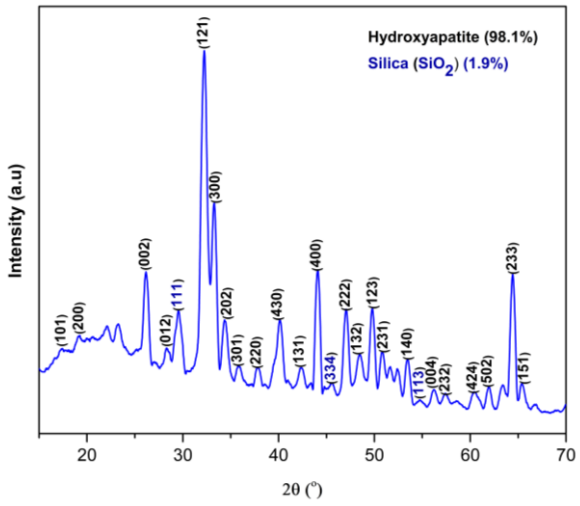

Fig. 7. Diffraction pattern of hydroxyapatite/SiO_2/gelatin scaffolds

3.9. Characterization of hydroxyapatite with electron microscopy spectroscopy (SEM)

Scanning Electron Microscopy (SEM) testing aimed to determine the differences in morphological characteristics and micropore size of hydroxyapatite with hydroxyapatite/SiO_2/gelatin scaffold composites. The characteristics of hydroxyapatite samples in Fig. 8 showed that the hydroxyapatite obtained produced a granular, uniform, irregular morphology with pore sizes in the range of 1.04–

1.93µm. SEM results showed that the synthesis of hydroxyapatite with this precipitation method produced good results. The results obtained are supported by the research of Sari et al. [23], who, in their research, produced granule-shaped hydroxyapatite with uniform grains. In addition, the irregular morphological shape of hydroxyapatite has been reported in the research of Ferreira et al. [36].

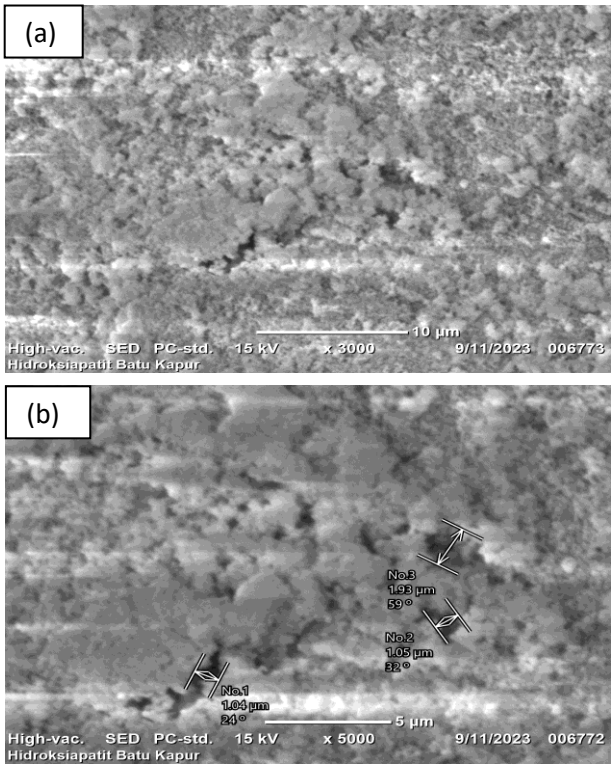

Fig. 8. SEM results of limestone hydroxyapatite (a) 3000x magnification (b) 5000x magnification

3.10. Characterization of hydroxyapatite with electron microscopy spectroscopy (SEM)

SEM characterization aimed to determine the surface morphology, structure, and pore size formed in hydroxyapatite/SiO_2/gelatin scaffold samples produced by the freeze-dryer method. The analysis in Fig. 9 showed that the sample formed a pore with a pore size found in the range of 155-218µm or an average of 188µm. The resulted pores can provide an ideal environment for bone cell proliferation during the bone regeneration process. The pore size of about >100µm plays an important role in accelerating the process of cell and ion transport in the application of scaffolds for bone regeneration [3]. This result is supported by the research of Iga et al. [37], which produced scaffold pores in the range of 150–500µm suitable for bone tissue regeneration. Research by Mohonta et al. [38] produced pore sizes on nHAp/CS/Gelatin-based scaffolds with an average pore size of 180µm, considered ideal for tissue growth and can also perform osteoinduction and osteointegration in the bone regeneration process.

The resulted pore size increased upon the addition of gelatin to the composite, where the range of hydroxyapatite pores was around 1.04–1.93µm, then increasing to 155-218µm after being composited as a scaffold. The use of gelatin in this study showed that gelatin could increase the porosity and pore size of the scaffold because gelatin is a biopolymer that can build a porous structure, causing an increase in surface area and open space that can be beneficial for nutrient delivery and cell growth in bone defects [3]. Gelatin has a high surface activity for being hydrophilic and hydrophobic and having many polypeptide chains arranged in a three-dimensional structure [21]. In addition, this highly porous scaffold structure was produced by the freeze-dryer method because, when using this technique, water molecules formed ice crystals during freezing. Afterward, the water was removed by freeze-drying through a sublimation process. Finally, a porous scaffold was formed where the pore boundaries were visible as particles trapped in the matrix throughout the scaffold [38].

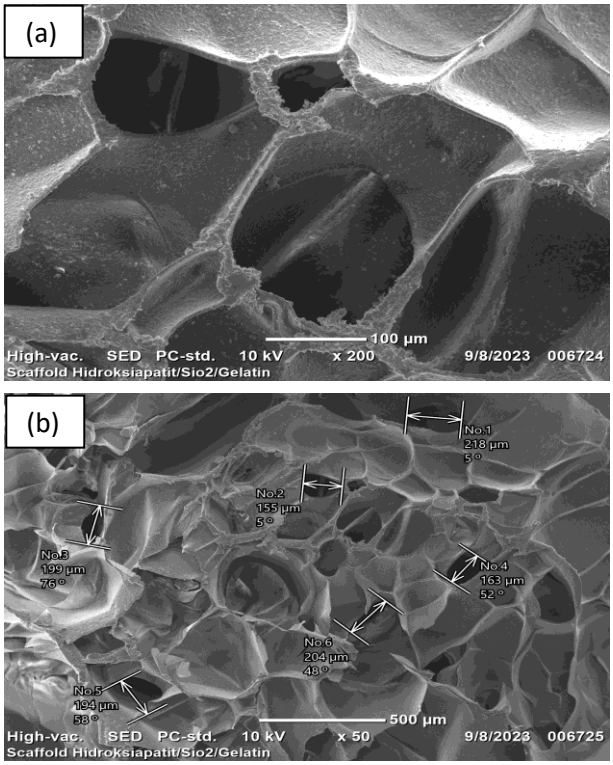

Fig. 9. SEM results of hydroxyapatite/SiO_2/gelatin (a) 50x magnification (b) 200x magnification

3.11. Mechanical test

The mechanical properties of scaffolds are one of the most important parameters in tissue engineering because appropriate mechanical properties can provide a suitable environment for cell attachment, proliferation, and differentiation [39]. In this study, the mechanical properties of the scaffold were generated from the analysis of the compressive strength test using a universal testing machine. The compressive strength value of the hydroxyapatite/ SiO_2/gelatin scaffold obtained was around 1.71 MPa. This value is in accordance with the standard suitable for bone regeneration, around 1–10 MPa [40]. Similar results have also been reported by Mohonta et al. [38], who produced nHAp/Cs/Gel scaffolds with a value of 1.76 MPa. Even though the mechanical properties of this composite were lower, the presence of SiO_2 in this composite could stimulate bone growth more than the addition of chitosan. This is because SiO_2 is osteoinductive, which can induce faster bone formation in materials such as apatite. SiO_2 also has good

bioactivity, so it can increase the bioactivity of the scaffold [10]. Apart from that, SiO_2 also has a porous structure with a large surface area, which supports its application as a bone scaffold [41].

The improvement in the mechanical properties of scaffolds in this study was supported by the addition of SiO_2. This has also been proven by research Taha et al. [42] in which the addition of SiO_2 to CHA caused an increase in the mechanical properties of nanocomposites. The compressive strength value obtained tended to approach the lowest limit of the standard scaffold compressive strength value due to the relatively low concentration of SiO_2 used. Furthermore, the kind and quantity of coexisting phases, the existence or absence of chemical interactions between the constituents, the adhesion of good or poor components, and the homogeneity of the material's microstructure are the primary factors determining the mechanical properties of composites [43].

3.12. Porosity test

Porosity is an important factor in scaffold characterization as it serves to facilitate cell migration, blood circulation, and vascular processes [44]. The porosity of the scaffold in this study was determined by the liquid displacement method. The porosity result obtained was 75%. Similar results have been reported by research Tomic et al. [45], which obtained scaffold porosity in the range of 72.10–84.25% in hydrogel-based scaffolds. It has been shown that composite scaffolds possessing a porosity exceeding 60% can efficiently stimulate osteogenic differentiation, cell proliferation, and bone repair [5]. There exists a considerable correlation between the mechanical properties of the scaffold and its porosity level [46].

4. Conclusion

Hydroxyapatite has been successfully synthesized using limestone as a calcium precursor. This was evidenced by the results of characterization using FTIR, XRD, and SEM. Hydroxyapatite was made into scaffolds with the addition of SiO_2 and gelatin. The addition of SiO_2 increased the compressive strength value of the scaffold so that it reached the existing scaffold compressive strength standard. The addition of gelatin has been proven to increase the pore size and porosity of the scaffold. Based on the results obtained, the hydroxyapatite/SiO_2/gelatin scaffold has fulfilled the standards as a bone scaffold candidate.

Acknowledgments

We are grateful for the support from the research laboratory of Makassar State University and the inorganic laboratory of Hasanuddin University for this research. In addition, grant funds with contract number 00323/UN4.22/PT.01.03/2023 from the Institute for Research and Community Service of Hasanuddin University through the Collaborative Fundamental Research Plan for Fiscal Year 2023 were also used to support this research.

References

1. R. Zhao, T. Shang, B. Yuan, X. Zhu, X. Zhang, and X. Yang, *Osteoporotic Bone Recovery by A Bamboo-Structured Bioceramic with Controlled Release of Hydroxyapatite Nanoparticles,* Bioactive Materials. 17 (2022) 379–393.
2. S.I Mostafa, N.M. Abdelfattah, S.M. Ghorab, M.F. Osman, and N.A. Elwassefy*, Bone Regeneration by Hydroxyapatite-Gelatin nanocomposites*, Research Square. (2022) 2-21.
3. T. Ju, Z. Zhao, L. Ma, W. Li, S. Li, and J. Zhang, *Cyclic Adenosine Monophosphate-Enhanced Calvarial Regeneration by Bone Marrow-Derived Mesenchymal Stem Cells on a Hydroxyapatite/Gelatin Scaffold,* ACS Omega. 6 (2021) 13684–13694.
4. B.C.You, C.E Meng, N.F.M. Nasir, E.Z.M. Tarmizi, K.S. Fhan, E.S. Kheng, et al, *Dielectric and Biodegradation Properties of Biodegradable Nano-Hydroxyapatite/Starch Bone Scaffold*, Journal of Materials Research and Technology. 18 (2022) 3215–3226.
5. P. Ma, W. Wu, Y. Wei, L. Ren, S. Lin, and J. Wu, *Biomimetic Gelatin/Chitosan/Polyvinyl Alcohol/Nano-Hydroxyapatite Scaffolds for Bone Tissue Engineering*, Materials and Design. 207 109865 (2021) 1-11.
6. A. Nihmath and M.T. Ramesan, *Fabrication, Characterization, and Dielectric Studies of NBR/Hydroxyapatite Nanocomposite*s, J. Inorg Organomet Polym. (2016).
7. K. Sinulingga, M. Sirait, N. Siregar, and H. Abdullah, *Synthesis and Characterizations of Natural Limestone-Derived Nano-Hydroxyapatite (Hap): A Comparison Study of Different Metal-Doped Haps on Antibacterial Activity*, Royal Society of Chemistry. 11 (2021) 5896–15904.
8. C.G Kim, K.S. Han, S. Lee, M.C. Kim, S.Y. Kim, and J. Nah, *Fabrication of Biocompatible Polycaprolactone-Hydroxyapatite Composite Filaments for the FDM 3D Printing of Bone Scaffolds,* Applied Sciences. 11 6351 (2021) 1–9.
9. R.C.D.O Ponciano, A.C.F.D.M. Costa, R.C. Barbosa, M.V.L. Fook, and J.J. Ponciano, *Chitosan and Hydroxyapatite Scaffolds with Amoxicillin for Bone Repair*, Research and Development. 10 5 (2021) 1-16.
10. L. Liu, X. Ni, X. Xiong, J. Ma, and X. Zeng, *Low Temperature Preparation of SiO_2 Reinforced Hydroxyapatite Coating on Carbon/Carbon Composites,* Journal of Alloy and Compounds. 788 (2019) 798-778.
11. A. Sajjad, W.Z.W. Bakar, D. Mohamad, and T.P. Kannan, *Characterization and Enhancement of Physico-Mechanical Properties of Glass Ionomer Cement by Incorporating a Novel Nano Zirconia Silica Hydroxyapatite Composite Synthesized Via Sol-Gel*, AIMS Materials Science. 6 5 (2019) 730–747.
12. M. Monavari, S. Homaeigohar, M.F. Chandia, Q. Nawaz, M. Monavari, A. Venkatraman, et al, *3D Printing of Alginate Dialdehyde-Gelatin (ADA-GEL) Hydrogels Incorporating Phytotherapeutic Icariin Loaded Mesoporous SiO_2-CaO Nanoparticles for Bone Tissue Engineering,* Material Science and Engineering C. 131 112470 (2021) 1-11.
13. A. Akhtar, V.F. Rad, A.R. Moradi, M.Yar, and M. Bazzar, *Emerging Polymeric Biomaterials and Manufacturing-Based Tissue Engineering Approaches for Neuro Regeneration-A Critical Review on Recent Effective Approaches,* Smart Material in Medicine. 4 (2023) 337–355.
14. A.R. Noviyanti, Haryono, R. Pandu, dan D.R. Eddy, *Cangkang Telur Ayam sebagai Sumber Kalsium dalam Pembuatan Hidroksiapatit untuk Aplikasi Graft Tulang*, Chemica at Natura Acta. 5 3 (2017) 107–111.
15. M. Mozartha, M. Praziandithe, dan Sulistiawati. *Pengaruh Penambahan Hidroksiapatit dari Cangkang Telur terhadap Kekuatan Tekan Glass Ionomer Cement*, Jurnal B-Dent. 2 1 (2015) 75–81.
16. M. Khalid, S.S.B. Jikan, S. Adzila, Z. Murni, N.A. Badarulzaman, R. Rosley, et al, *Synthesis and Characterizations of Hydroxyapatite using Precursor Extracted from Chicken Egg Shell Waste,* Biointerface

Research in Applied Chemistry. 4 (2022) 5663–5671.

17. S.M. Mangkuasih dan L. Rohmawati, *Sintesis Hidroksiapatit dari Tulang Ikan Sapu-Sapu (Hypostomus plecostomus) dengan Metode Presipitasi,* Jurnal Teori dan Aplikasi Fisika. 9 2 (2021) 229–236.
18. Y.D.S Yudyanto and Hartatiek, *Pengaruh Nanosilika terhadap Kekerasan dan Porositas Nanokomposit HA-SiO2 Berbasis Batuan Onyx Bojonegoro,* Journal of Physical Science and Engineering. 1 1 (2016) 13-18.
19. F. Afriani, Y. Tiandho, Evi J, A. Indriawati, and R.A. Rafsanjani, *Synthesis and Characterization of Hydroxyapatite/Silica Composites Based on Cockle Shells Waste and Tin Tailings,* IOP Conf. Series: Earth and Environmental Science. 353 012032 (2019) 1–5.
20. K. Maji and S. Dasgupta, *Hydroxyapatite-Chitosan and Gelatin Based Scaffold for Bone Tissue Engineering*, The Indian Ceramic Society. 73 2 (2014) 110–114.
21. Q. Sun, L. Yu, Z. Zhang, C. Qian, H. Fang, J.Wang, et al, *A Novel Gelatin/Carboxymethyl Chitosan/Nano-Hydroxyapatite/B-Tricalcium Phosphate Biomimetic Nanocomposite Scaffold for Bone Tissue Engineering Applications*, Frontiers in Chemistry. (2022) 1–12.
22. N.A.S.M. Pu'ad, P. Koshy, H.Z. Abdullah, M.I. Idris, and T.C. Lee, *Synthesis of Hydroxyapatite from Natural Sources*, Heliyon. 5 (2019) 1–14.
23. M. Sari, P. Hening, I.D. Ana, and Y. Yusuf, *Bioceramic Hydroxyapatite-Based Scaffold With a Porous Structure using Honeycomb As A Natural Polymeric Porogen for Bone Tissue Engineering,* Biomaterials Research. 25 2 (2021) 1–13.
24. J. Klinkaewnarong and S.Utarab, *Ultrasonic-Assisted Conversion of Limestone into Needle-Like Hydroxyapatite Nanoparticles*, Ultrasonics Sonochemistry. (2018) 1-38.
25. C.S. Kumar, K. Dhanaraj, R.M. Vimalathithan, P. Ilaiyaraja, and G. Suresh, *Hydroxyapatite for Bone Related Applications Derived from Sea Shell Waste by Simpleprecipitation Method*, Journal of Asian Ceramic Societies. 8 2 (2020) 416–429.
26. Z. Emami, M. Ehsani, M. Zandi, H. Daemi, M.H. Ghanianc, and R. Foudazi, *Modified Hydroxyapatite Nanoparticles Reinforced Nanocomposite Hydrogels Based on Gelatin/Oxidized Alginate Via Schiff Base Reaction,* Carbohydrate Polimer Technologies Applications. 2 100056 (2021) 1–10.
27. M. Sirait, K. Sinulingga, N. Siregar, and R.S.D Siregar, *Synthesis of Hydroxyapatite from Limestone by using Precipitation Method*, Journal of Physics: Conference Series. 1462 (2020) 1–8.
28. K.A. Pridanti, F. Cahyaraeni, E. Harijanto, Soebagijo, D. Rianti, W. Kristanto, et al, *Characteristics and Cytotoxicity of Hydroxyapatite from Padalarang-Cirebon Limestone as Bone Grafting Candidate*, Biochem Cell Arch. 20 2 (2020) 4727–4731.
29. I. Raya, E. Mayasari, A. Yahya, M. Syahrul, and A.I. Latunra, *Synthesis and Characterizations of Calcium Hydroxyapatite Derived from Crabs Shells (Portunus pelagicus) and Its Potency in Safeguard against to Dental Demineralizations*, International Journal of Biomaterials. (2015) 1–8.
30. K. Sinulingga, M. Sirait, N. Siregar, and H. Abdullah, *Synthesis and Characterizations of Natural Limestone-Derived Nano-Hydroxyapatite (HAp): A Comparison Study of Different Metals Doped Haps on Antibacterial Activity*, Royal Society of Chemistry. 11 (2021) 5896–15904.
31. P.P. Nayak and A.K. Datta, *Synthesis of SiO_2-Nanoparticles from Rice Husk Ash and its Comparison with Commercial Amorphous Silica through Material Characterization,* Silicon. (2020).
32. P.H. Nazopatul, Irmansyah, and Irzaman, *Extraction and Characterization of Silicon Dioxide from Rice Straw,* IOP Conf. Series: Earth and Environmental Science. 209 012013 (2018) 1–5.
33. N. Ismail, M.I. Idris, and H.Z. Abdullah, *Effects of Ultraviolet (UV) Treatment on the Properties of Black Tilapia Fish Skins Gelatin*, Materials Science Forum. 1010 (2020) 465–470.
34. M. Wahyuningtyas, N. Jadid, P. Burhan, and L. Atmaja, *Physical and Chemical Properties of Gelatin from Red Snapper Scales: Temperature Effects*, Jurnal Teknik ITS. 8 2 (2019) 95–101.
35. Seyedmajidi, Seyedali, and M. Seyedmajidi, *Fluoroapatite: A Review of Synthesis, Properties and Medical Applications vs Hydroxyapatite,* Iranian Journal of Material Science and Engineering. 19 2 (2022) 1-20.
36. C.R.D. Ferreira, A.G. Santiago, R.C. Vasconcelos, D.F.F. Paiva, F.Q. Pirih, A.A. Araujo, et al, *Study of Microstructural, Mechanical, and Biomedical Properties of Zirconia/Hydroxyapatite Ceramic Composites,* Ceramic International. 48 (2022) 12376–12386.
37. C. Iga, S. Paweł, L. Marcin, and K.L. Justyna, *Polyurethane Composite Scaffolds Modified with the Mixture of Gelatin and Hydroxyapatite Characterized by Improved Calcium Depositio,.* Polymers. 12 410 (2020) 1-18.
38. S.K. Mohonta, K.H. Maria., S. Rahman, H. Das, and S.M. Hoque, *Synthesis of Hydroxyapatite Nanoparticle and Role of its Size in Hydroxyapatite/Chitosan-Gelatin Biocomposite for Bone Grafting,* International Nano Letters. (2021).
39. M. Ahmadipour, H. Mohammadi, A.L. Pang, M. Arjmand, T.A. Otitoju, P.U. Okoye, and B. Rajitha, *A Review: Silicate Ceramic-Polymer Composite Scaffold for Bone Tissue Engineering*, International Journal of Polymeric Materials And Polymeric Biomaterials. (2020) 1–14.
40. J. Zheng, Z. Zhao, Y. Yang, S. Wang, Y. Zhao, Y. Xiong, et al, *Biphasic Mineralized Collagen-Based Composite Scaffold for Cranial Bone Regeneration In Developing Sheep*, Regenerative Biomaterials. 9 (2020) 1–14.
41. D.R. Wicakso, A. Mirwan, E. Agustin, N.F. Nopembriani, I. Firdaus, and M. Fadilla, Potential of silica from water treatment sludge modified with chitosan for Pb(II) and color adsorption in sasirangan waste solution, Commun. Sci. Technol. 7 2 (2022) 188-193.
42. M.A. Taha, R.A. Youness, and M. Ibrahim, *Biocompatibility, Physico-Chemical and Mechanical Properties of Hydroxyapatite-Based Silicon Dioxide Nanocomposites for Biomedical Applications,* Ceramic International. (2020) 1–12.
43. J. Czechowska, E. Cicho, A. Belcarz, A. Siosarczyk, and A. Zima, *Effect of Gold Nanoparticles and Silicon on the Bioactivity and Antibacterial Properties of Hydroxyapatite/Chitosan/Tricalcium Phosphate-Based Biomicroconcretes,* Materials. 14 3854 (2021) 1–15.
44. S.A. Reina, B.J.E. Tito, M.H. Malini, F.G. Iqrimatien, Esa'diyah, and Aminatun, *Porosity and Compressive Strength of PLA-Based Scaffold Coated With Hydroxyapatite-Gelatin to Reconstruct Mandibula: A Literature Review,* Journal of Physics: Conference Series. 1816 012085 (2021) 1-6.
45. S.L. Tomic, J.N. Runic, M. Vukomanovic, M.M. Babic, and J.S. Vukovic, *Novel Hydrogel Scaffolds Based on Alginate, Gelatin, 2-hydroxyethyl Methacrylate, and Hydroxyapatite,* Polymers. 13 932 (2021) 1-16.
46. D, Atila, A. Karatas, A. Evcin, D. Keskin, and A. Tezcaner, *Bacterial Cellulose-Reinforced Boron-Doped Hydroxyapatite/Gelatin Scaffolds for Bone Tissue Engineering*, Cellulose. (2019).